# Mussel-Inspired Electrospun Smart Magnetic Nanofibers for Hyperthermic Chemotherapy

*Amin GhavamiNejad, Arathyram Ramachandra Kurup Sasikala, Afeesh Rajan Unnithan, Reju George Thomas, Yong Yeon Jeong, Mohammad Vatankhah-Varnoosfaderani, Florian J. Stadler,* Chan Hee Park,* and Cheol Sang Kim**

**A method for the versatile synthesis of novel, mussel-inspired, electrospun nanofibers with catechol moieties is reported. These mussel-inspired nanofibers are used to bind iron oxide nanoparticles (IONPs) and the borate-containing anticancer drug Bortezomib (BTZ) through a catechol metal binding mechanism adapted from nature. These smart nanofibers exhibit a unique conjugation of Bortezomib to their 1, 2-benzenediol (catechol) moieties for enabling a pH-dependent drug delivery towards the cancer cells and the IONPs via strong coordination bonds for exploiting the repeated application of hyperthermia. Thus the synergistic anticancer effect of these mussel-inspired magnetic nanofibers were tested in vitro for the repeated application of hyperthermia along with the chemotherapy and found that the drug-bound catecholic magnetic nanofibers exhibited excellent therapeutic efficacy for potential anticancer treatment.**

Dr. A. GhavamiNejad, A. R. K. Sasikala, Dr. A. R. Unnithan, Prof. C. H. Park, Prof. C. S. Kim
Department of Bionanosystem Engineering
Graduate School
Chonbuk National University
Jeonju 561–756, Republic of Korea
E-mail: biochan@jbnu.ac.kr; chskim@jbnu.ac.kr
Dr. A. R. Unnithan, Prof. C. H. Park, Prof. C. S. Kim
Mechanical Design Engineering
Chonbuk National University
Jeonju 561–756, Republic of Korea
R. G. Thomas, Prof. Y. Y. Jeong
Department of Radiology
Chonnam National University Hwasun Hospital
Chonnam National University Medical School
Gwangju 501–746, Republic of Korea
Dr. M. Vatankhah-Varnoosfaderani
Department of Chemistry
University of North Carolina
Chapel Hill, NC 27599–3290, USA
Prof. F. J. Stadler
College of Materials Science and Engineering
Shenzhen University
Shenzhen 518060, PR China
E-mail: fjstadler@szu.edu.cn
Prof. F. J. Stadler
Nanshan District Key Lab for Biopolymers and Safety Evaluation
Shenzhen 518060, PR China
Prof. F. J. Stadler
Shenzhen Key Laboratory of Special Functional Materials
Shenzhen 518060, PR China

**DOI: 10.1002/adfm.201500389**

## 1. Introduction

Hyperthermia has often been used in multimodality strategies, as it can synergistically enhance the antitumor effects of chemotherapy, radiotherapy, and immunotherapy.[1] The major technical challenge in hyperthermia treatment is locally heating the tumor region to the desired temperature without overheating the surrounding healthy tissues. Recently, there has been an increased level of interest in the use of nanofibers loaded with iron oxide nanoparticles (IONPs) for cancer therapy.[2,3] The main advantage of such magnetic fibers is the local and precise delivery of the IONPs, which is ideal for the hyperthermic treatment of easily accessible tumors. The development of a material that could enable repeated heating upon the application of an alternating magnetic field (AMF) and controlled drug delivery in a cancer environment would make the use of these magnetic fibers highly useful for the combined application of hyperthermia treatment and chemotherapy.

In many reports, composite nanofibers were synthesized from a dispersion of previously prepared nanoparticles in a polymer solution;[2,4] however, it is difficult to homogeneously mix such small nanoparticles with macromolecules in an organic phase for an electrospinning process due to their tendency to aggregate and precipitate.[5] As a result, the controlled assembly of nanoparticles onto the nanofibers could be a good strategy not only for preventing these aggregations, but also for increasing the chance of loading more nanoparticles onto the surface due to the large surface area of the electrospun nanofibers.[6,7]

It has been reported by many researchers that 3,4-dihydroxyphenylalanine (Dopa) is capable of strong interactions with metal oxides.[8] Surface modification of various materials containing polydopamine via a simple immersion method is a facile strategy that can significantly alter surface properties, enabling interaction with metal oxides.[9] This method is based on the self-polymerization of dopamine under alkaline conditions, thus, changing catechol moieties to their oxidized forms.[10] Due to this oxidation, the formed catechol-coated surface exhibits low cell attachment and does not show any pH-dependent binding.[11] Recent studies explored the use of non-oxidized dopamine to enhance the adhesion and migration

of cells.[12] In addition to the strong binding ability of catechol groups to metal oxides, previous studies have demonstrated that catechol groups can be utilized to bind and release borate-containing anticancer drugs such as Bortezomib (BTZ) in a pH-dependent manner.[14]

Here we report the first versatile synthesis of novel catechol moieties on electrospun nanofibers for binding IONPs and the borate-containing anticancer drug BTZ by means of a catechol–metal binding mechanism first observed naturally in mussels. The present study aims to develop smart magnetic nanofibers that are capable of both pH-dependent drug release in a cancer environment and heat generation under the application of a magnetic field for the combined treatments of hyperthermia and chemotherapy.

## 2. Results and Discussion

The novel catecholic nanofibers were fabricated by electrospinning a mussel-inspired copolymer, poly(methyl methacrylate-*co*-dopamine methacrylamide) p(MMA-*co*-DMA) (further abbreviated as MADO), synthesized via reversible addition–fragmentation chain transfer (RAFT) polymerization. IONPs were synthesized as reported elsewhere[15] and introduced to the MADO nanofibers to initiate the process of catechol–metal binding. For the proof of concept, MADO nanofibers were carefully immersed into the $Fe_3O_4$ solution. In order to utilize the catecholic–metal conjugation, the pH of the aqueous solution was adjusted to 8.5 as the optimum for the present study. The nanoparticles interacted with the surfaces of the MADO nanofibers as the pH increased, leading to a color change of the fiber mats from white to brown. In contrast, no color changes were observed for the pure poly(methyl methacrylate) (PMMA) nanofibers, confirming that the absorption of the magnetic nanoparticles was driven by the catechol moiety in MADO. The as-obtained magnetic nanofibers are abbreviated as MADO–$Fe_3O_4$. In order to enable multimodal treatment combining hyperthermia and chemotherapy, BTZ-loaded MADO–$Fe_3O_4$ nanofibers (MADO–$Fe_3O_4$–BTZ) were also prepared and used for the application of hyperthermic chemotherapy.

High-resolution transmission electron microscopy (HRTEM) demonstrated that the as-prepared IONPs were homogenously distributed with an average diameter of less than 20 nm (Figure S3 in the Supporting Information, SI). All diffraction peaks present in the x-ray diffraction (XRD) spectrum of the as-prepared IONPs (Figure S4, SI) were in agreement with the standard diffraction card, JCPDS No. 19–062 (JCPDS = Joint Committee on Powder Diffraction Standards).[7] The morphologies of the MADO, MADO–$Fe_3O_4$, and MADO–$Fe_3O_4$–BTZ nanofibers were analyzed using field-emission scanning electron microscopy (FESEM) and TEM (**Figure 1**). The MADO nanofibers were found to be smooth and uniform, with an average diameter of 800 nm (Figure 1A). The IONPs were selectively and uniformly dispersed on the surface of the polymeric nanofibers due to the presence of catechol groups on the nanofiber surface (Figure 1B). Also, introducing BTZ did not affect the morphology of MADO–$Fe_3O_4$ nanofibers (Figure 1C). The TEM image (Figure 1D) also confirmed the uniform distribution of IONPs on the nanofiber surface. These results showed

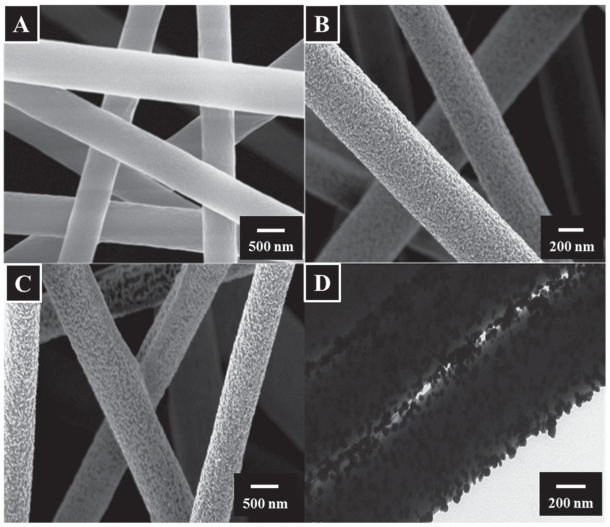


**Figure 1.** FESEM images of electrospun A) MADO nanofibers, B) MADO–$Fe_3O_4$ nanofibers, and C) MADO–$Fe_3O_4$–BTZ nanofibers; and D) TEM image of MADO–$Fe_3O_4$–BTZ nanofibers.

that the catecholic nanofibers possess very good morphology with an ability to bind with IONPs selectively and uniformly.

The quantity of the $Fe_3O_4$ attached to the nanofibers was determined via thermogravimetric analysis (TGA), as shown in **Figure 2**. Pure fiber was found to start decomposing around 382 °C. The decomposition temperature of the composite nanofibers was slightly higher than that of the pure fiber; this can be attributed to the interactions between the polymers and nanoparticles, which is supported by the slight improvement in the thermal stability of the composite fibers.[16] The organic parts of the samples are almost completely disintegrated at ≈500 °C, while the IONPs as well as the IONPs in the composite are nearly unaffected by the elevated temperature. As a result, the amount of nanoparticle in the nanocomposite fiber can be estimated from the residual mass of the composite, i.e., slightly below 11%.

The Raman spectroscopy peaks (**Figure 3**) at 590 and 640 $cm^{-1}$ are assigned to the vibrations of the oxygen–metal

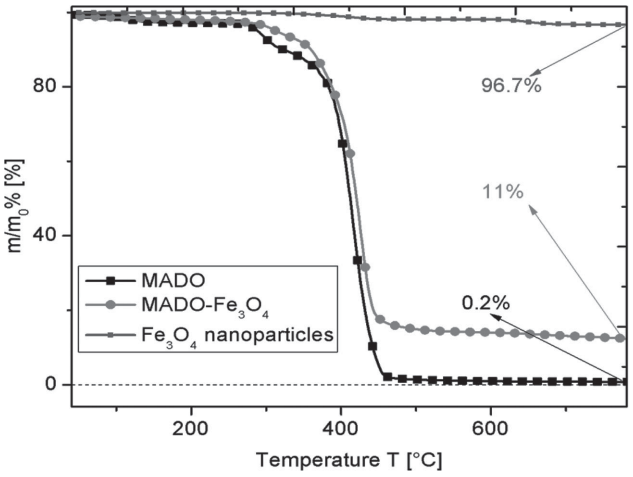


**Figure 2.** TGA of $Fe_3O_4$ nanoparticles, MADO, and MADO–$Fe_3O_4$. Current and initial sample mass are indicated by $m$ and $m_0$, respectively.

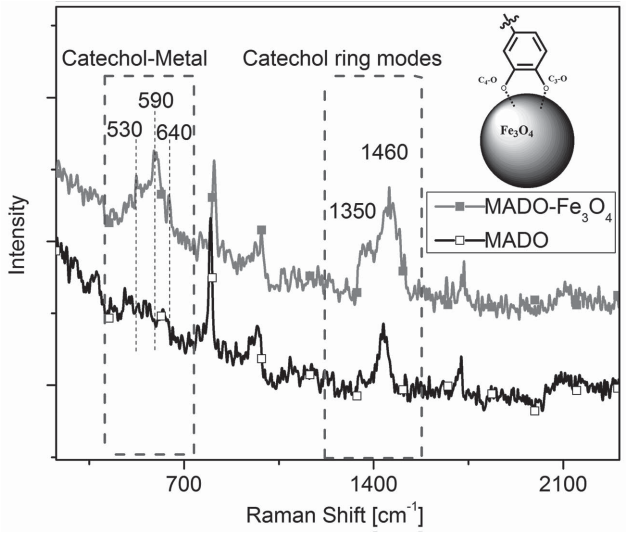


**Figure 3.** Resonance Raman spectra of MADO and MADO–$Fe_3O_4$ nanofibers.

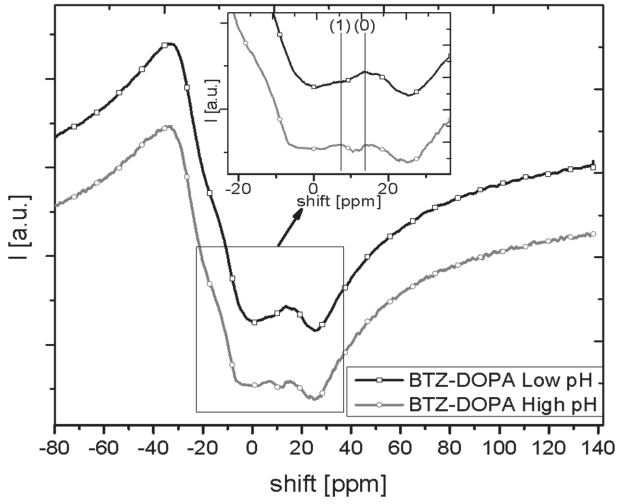


**Figure 4.** $^{11}$B-NMR spectra of BTZ with the addition of dopamine hydrochloride at various pH values. *I* represents intensity.

chelate bonds, namely by the oxygen coordination on $C_3$ and $C_4$ of the catechol ring. This proves that the interaction between nanofiber and nanoparticles is through the metal–catechol complexation.[17] According to previous studies,[18] bidentate coordination and the resulting charge transfer cause the peak at 530 $cm^{-1}$—though our signal strength is comparatively weaker, possibly due to the higher amount of monodentate coordination between catechol and $Fe_3O_4$ metal particles.[19] Higher-energy resonance peaks (1200–1500 $cm^{-1}$) have been assigned to catechol ring vibrations. The pronounced spectral features in this region highlight the involvement of the catechol in the interfacial charge transfer upon coordination with $Fe_3O_4$. The obtained results confirmed that Dopa-containing polymers can strongly bind to metal oxides.[20] X-ray photoelectron spectroscopy (XPS) and Fourier-transform IR (FTIR) were performed to further investigate the binding of MADO and IONPs, and the results fully confirmed the binding of IONPs on the surface of catecholic nanofibers (Figure S5–6, SI).

To confirm the interaction between BTZ and catechol groups in MADO–$Fe_3O_4$–BTZ, the change in the $^{11}$B-NMR spectra of BTZ following the addition of dopamine hydrochloride was investigated at various pH values. As shown in **Figure 4**, the $^{11}$B-NMR spectrum of this mixture at pH 5 reveals a peak at 13.2 ppm, indicating the presence of uncomplexed BTZ. By adding NaOH solution (1 N) and increasing the pH of the solution to 7.5, the peak from free or unreacted BTZ (marked as 0 in spectrum) at a chemical shift of 13.2 ppm decreases, while a peak at a chemical shift of 9.2 ppm grows in intensity (marked as 1 in spectrum), indicating the formation of boron–Dopa complexation.[21] To obtain higher resolution in the $^{11}$B NMR spectrum, we used 4-vinyl phenyl boronic acid (VPBA) as an analogue of BTZ and monitored the catechol–VPBA binding (Figure S2, SI); the same trend was observed.

Field-dependent magnetic measurements of the as-synthesized $Fe_3O_4$ nanoparticles and the MADO–$Fe_3O_4$ nanofibers were carried out (**Figure 5**). Hysteresis was not observed in the magnetization curves of the $Fe_3O_4$ and MADO–$Fe_3O_4$ nanofibers, indicating superparamagnetic characteristics. Moreover, the absence of coercivity or remanence further confirmed the superparamagnetic behavior of these samples. The saturation magnetization values ($M_s$) of $Fe_3O_4$ and MADO–$Fe_3O_4$ nanofibers at room temperature (300 K) were found to be 83.9 and 74.6 emu $g^{-1}$, respectively. There is only a small reduction in saturation magnetization values in comparison to pure IONPs due to the well-dispersed state of the IONPs with minimum aggregation on the MADO–$Fe_3O_4$ nanofibers. Therefore, MADO–$Fe_3O_4$ nanofibers exhibiting superparamagnetic behavior with high saturation magnetization values are a promising material for applications in hyperthermia treatments.[4]

Magnetic-nanoparticle-mediated hyperthermia utilizes the heating ability of superparamagnetic IONPs under the application of an AMF.[22] The AMF-induced heating ability of IONPs

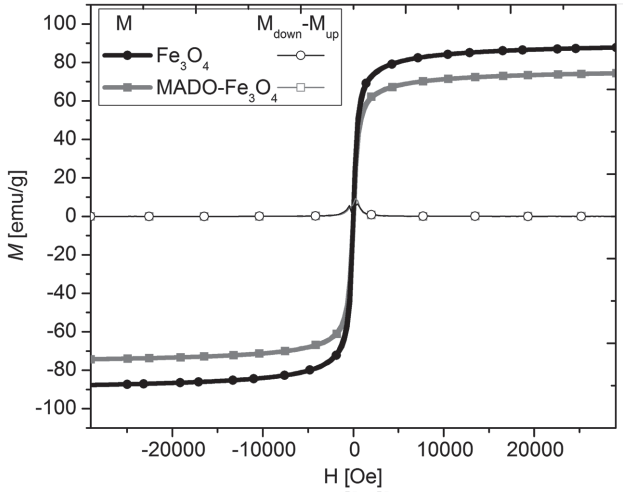


**Figure 5.** Magnetic hysteresis curves of $Fe_3O_4$ and MADO–$Fe_3O_4$. *M* and *H* represents the magnetization and the magnetic field, respectively. In the legend, M refers to the iron metal centers, and $M_{up}$ and $M_{down}$ indicate the situation where the iron centers have alternating opposite spins.

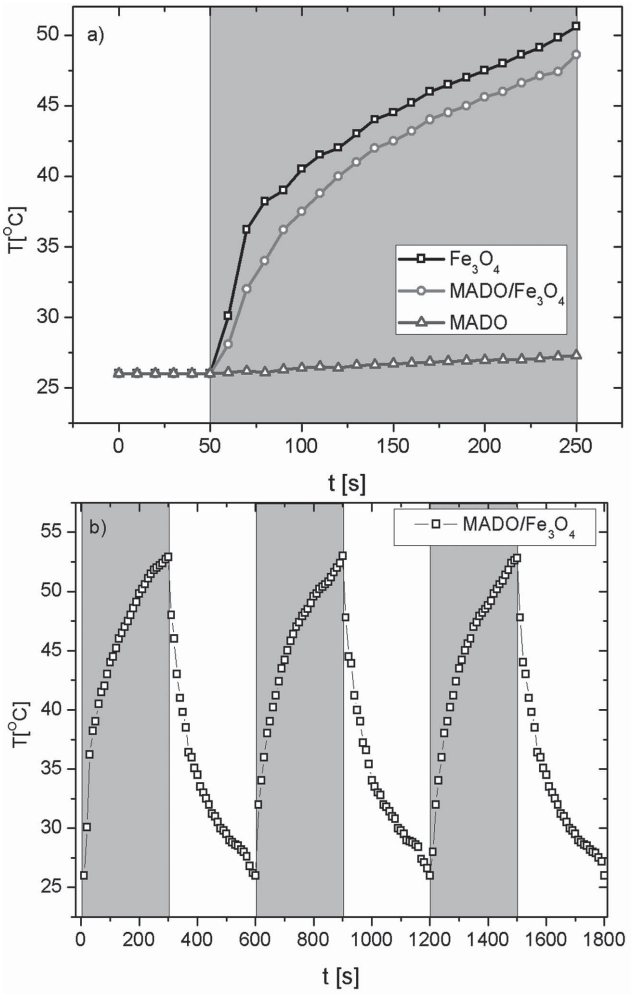


**Figure 6.** Temperature (*T*)–time (*t*) profile obtained a) upon the application of an AMF, and b) with and without the application of the magnetic field; the shaded zones indicate the application of the magnetic field.

with diameters below 20 nm arises primarily from relaxation loss (including Néel and Brownian relaxation).[23] The heating profiles of the $Fe_3O_4$, MADO–$Fe_3O_4$, and MADO (control) fibers were studied at an AMF strength of 12.57 Oe and a frequency of 293 kHz, and they are plotted as a function of time in **Figure 6**A. $Fe_3O_4$ and MADO–$Fe_3O_4$ nanofibers exhibited a drastic increase in heating ability compared to the control MADO nanofibers, which can be explained from the amount of superparamagnetic IONPs present in the sample. With detailed analysis, there is a small discrepancy in the heating efficiency of $Fe_3O_4$ and MADO–$Fe_3O_4$ nanofibers. This may be due to the reduction in the exposed surface area of the attached IONPs on the surface of the fibers. These results indicate a strong heating capacity for $Fe_3O_4$ and MADO–$Fe_3O_4$ nanofibers. In order to quantify the heating ability, the specific absorption rate (SAR) was measured. The SAR of as-prepared $Fe_3O_4$ was estimated to be 181.05 W $g^{-1}$ for an AMF of 12.57 Oe and a frequency of 293 kHz; this confirmed the strong heating ability.

In the case of cancer therapy, repeated application of hyperthermia is preferred along with other treatment modalities, as there is a chance of tumor metastasis. Most of the intravenously injected IONPs for hyperthermia treatment were rapidly cleared by the reticuloendothelial system, which may seriously affect the success rate. Hence, it is extremely beneficial to use a material that results in repeated heating of IONPs upon the application of AMF.[5] The repeated uniform heating and cooling profile of the MADO–$Fe_3O_4$ nanofibers was obtained in the presence and absence of an AMF (Figure 6B). The results indicated a uniform cyclic profile with a constant temperature rise, making it a very stable system for the application of hyperthermia treatment.

Biocompatibility of the material is an important factor for analysis before consideration for any clinical application. It is well known that $Fe_3O_4$ nanoparticles are promising candidates for biomedical application because of their excellent biocompatibility and stability in physiological environments.[24] The nanofiber biocompatibility was analyzed with a murine fibroblast (NIH3T3) cell line. The enhanced cell proliferation ability and biocompatibility of the MADO nanofibers were confirmed with an MTS assay (MTS = (3-(4,5-dimethylthiazol-2-yl)-5-(3-carboxymethoxyphenyl)-2-(4-sulfophenyl)-2H-tetrazolium); Figure S7, SI). The excellent biocompatibility and low cytotoxicity of dopamine contributed towards the enhanced cytocompatibility of the MADO nanofibers.[25]

pH-sensitive drug-delivery platforms have proven very efficient in cancer treatment.[14] Here we developed novel catechol nanofibers conjugated with the anticancer drug BTZ for pH-sensitive drug delivery specific to cancer cells, with the addition of hyperthermia treatment. In neutral or alkaline pH, BTZ and catechol form a stable boronate ester, rendering BTZ non-cytotoxic; meanwhile in a typical acidic cancer environment, the conjugation dissociates and BTZ is rapidly released, activating its proteasome-inhibiting function. The pH-dependent release of BTZ from the MADO nanofibers has been carried out at pH 7.4 and 5.0, with the maximum release of BTZ observed at low pH (pH = 5.0); the pH-triggered drug release from MADO–BTZ nanofibers is compared with physiological pH in the SI (Figure S9).

After confirming the biocompatibility and pH-dependent drug release, we further proceeded to evaluate the anticancer efficacy of the mussel-inspired catecholic magnetic nanofibers for the application of hyperthermia with chemotherapy. The independent hyperthermia and chemotherapeutic effects of the nanofibers as well as the combined effects were tested in vitro in MCF-7 (human breast cancer) and 4T1 (mouse mammary carcinoma) cell lines. The combined hyperthermia and chemotherapeutic effects were evaluated in MADO–$Fe_3O_4$–BTZ nanofibers under the application of an external magnetic field whereas the independent hyperthermia and chemotherapeutic effects were checked in MADO–$Fe_3O_4$ (AMF On) and MADO–BTZ (AMF Off) nanofibers. Based on the type of treatment, the samples were divided into two groups such as treated (with hyperthermia) and untreated (without hyperthermia) groups. In all experiments, the treated group received hyperthermia treatment for 10 min in a sterile environment whereas untreated samples were isolated in a mini-petri dish for the same period of time thereby cancelling out environmental effects on cell death. The cytotoxicity of cell lines was evaluated by an MTS assay. **Figure 7** shows the anticancer efficacy of the samples 24 h after hyperthermia treatment. According to the results, no

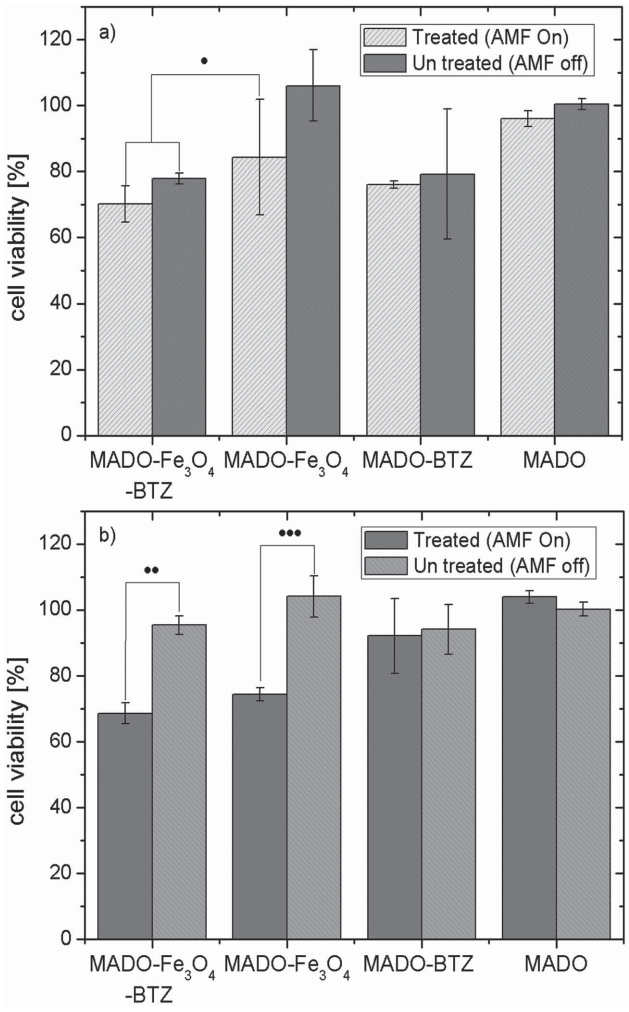


**Figure 7.** In-vitro anticancer effects of smart nanofibers in hyperthermia-treated and -untreated groups for the a) MCF-7 cell line and b) 4T1 cell line. Filled circles represent the values averages ± standard deviations (n = 3). P less than 0.05.

cell death was observed for the control MADO nanofibers, even after the hyperthermia treatment, which indicates that the field intensities are very safe and that there is no specific heating or other damaging effects from the AMF due to eddy-current heating of the cells. The anticancer effects of the MADO–$Fe_3O_4$, MADO–BTZ, and MADO–$Fe_3O_4$–BTZ nanofibers were measured from the increased cell death obtained from MTS assay. In the case of the MCF-7 cell line, cell death due to hyperthermia was only 11% in the MADO–$Fe_3O_4$ nanofibers, whereas the combined application of hyperthermia and chemotherapy in the MADO–$Fe_3O_4$–BTZ nanofibers resulted in a 30% increased toxicity (on average). In the case of the 4T1 cell line, cell death due to hyperthermia increased to around 29% in the MADO–$Fe_3O_4$ nanofibers whereas the combined application of hyperthermia and chemotherapy in the MADO–$Fe_3O_4$–BTZ resulted in approximately 35% cell death. Generally, the hyperthermia effect is more noticeable in highly proliferating cancer cell lines than it is in minimally proliferating cell lines. This may be due to the cell density factor and increased surface area contact with the IONPs. The proliferation characteristics of both cell lines are different, which in turn change their susceptibility to hyperthermia. These experiments also provided additional insights into the importance of cell attachment on the nanofiber for improved hyperthermia effects. In a detailed drug cytotoxicity analysis, MCF-7 cell line exhibited more susceptibility towards Bortezomib treatment compared to 4T1 cell line; nevertheless, the MADO–$Fe_3O_4$–BTZ group showed an increased anticancer effect on both cell lines along with the application of hyperthermia. This is due to the thermal enhancement of drug cytotoxicity in MADO–$Fe_3O_4$–BTZ, which resulted in a considerable anticancer effect.

Recently, several studies showed the enhancement of chemotherapeutic effects due to the concurrent application of hyperthermia;[26] thus, we hypothesize that our mussel-inspired catecholic nanofiber MADO–$Fe_3O_4$–BTZ would also exhibit an enhanced synergistic anticancer effect due to repeated hyperthermia cycles along with the drug toxicity. To further test our hypothesis, we undertook a repeated heating experiment with three cycles of AMF treatment on MADO–$Fe_3O_4$–BTZ nanofibers loaded with 4T1 cells keeping in mind the low drug susceptibility of the cells. Hyperthermia treatments were applied for three consecutive days, and the cell cytotoxicity was evaluated using an MTS assay 24 h after hyperthermia treatment (**Figure 8**). After the first hyperthermia cycle, we found that the cell viabilities (checked on day 2, i.e., 24 h after the first hyperthermia cycle) were reduced by 32%, whereas on day 3 and 4 (each checked 24 h after the most recent hyperthermia cycle) enhanced cell deaths of 57% and 80%, respectively, were observed.

In light of these experimental results, we conclude that the hypothesis, in which the repeated application of hyperthermia along with chemotherapy on MADO–$Fe_3O_4$–BTZ nanofibers results in a synergistic anticancer effect with few undesired side-effects, is indeed confirmed. These results indicate the excellent therapeutic efficacy of our novel drug-bound catecholic magnetic nanofibers MADO–$Fe_3O_4$–BTZ for potential anticancer therapy.

A live/dead viability/cytotoxicity assay (Molecular Probes, USA) was carried out to qualitatively analyze the anticancer

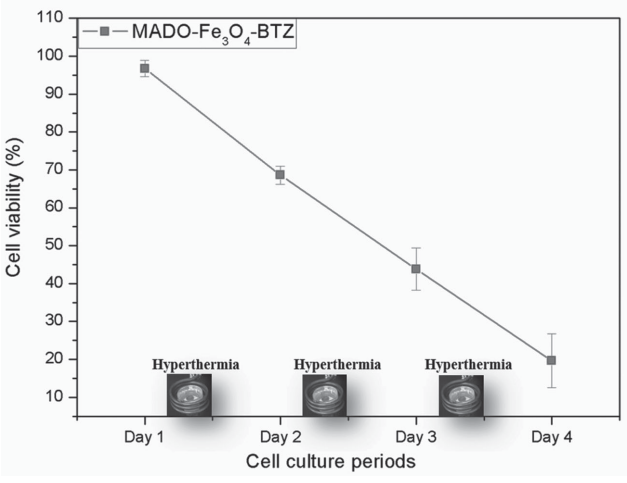


**Figure 8.** Anticancer effects of MADO–$Fe_3O_4$–BTZ on the 4T1 cell line under repeated application of hyperthermia on day 1, 2, and 3.

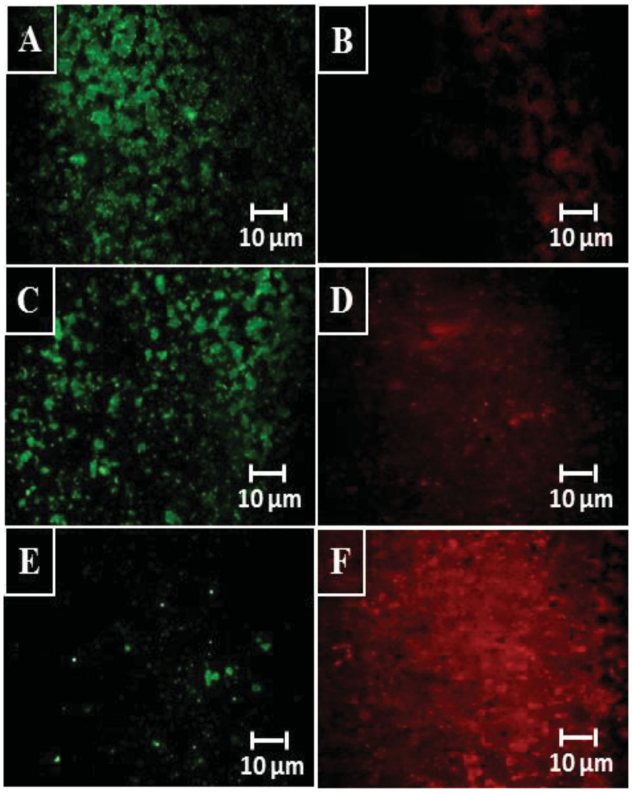


**Figure 9.** Live/dead assay displaying the cell viability after repeated hyperthermia treatments in MADO–$Fe_3O_4$–BTZ nanofibers. Cells 24 h after the A,B) first, C,D) second, and E,F) third cycle of hyperthermia treatment—that is on day 2 (A,B), 3 (C,D), and 4 (E,F). A, C, and E have calcein staining showing live cells; B, D, and F have ethidium homodimer staining showing dead cells.

efficacy of MADO–$Fe_3O_4$–BTZ. After the first hyperthermia treatment on day 1, a decrease of 30% viability was observed 24 h later (day 2). Cell death was further pronounced after repeated hyperthermia treatments, as demonstrated in **Figure 9**. On day 2, calcein-mediated green fluorescence was more visible in the live assay (Figure 9A) indicating a large number of intact, live cells, due to a high amount of calcein AM uptake. For the dead assay (Figure 9B), the red fluorescence intensity is very small due to only 30% cell death, indicated by slight ethidium homodimer uptake via the damaged cell membrane and nucleic acid attachment. Cell viabilities were further decreased considerably due to the repeated hyperthermia treatments on day 2 and 3 as indicated by the very low intensity of green fluorescence in the live assay (Figure 9C,E) and the very high intensity of red fluorescence in the dead assay (Figure 9D,F), confirming the strong anticancer efficacy of our MADO–$Fe_3O_4$–BTZ system for the synergistic application of hyperthermia and chemotherapy.

The nanofibers can be precisely introduced to the tumor region for hyperthermia treatment via a surgical or endoscopic method;[7] hence, imaging modality is vital for monitoring the implant (MADO–$Fe_3O_4$–BTZ) for repeated hyperthermia treatments. Magnetic resonance imaging (MRI) modality can monitor the implant with high spatial resolution and radiation-free, superior soft-tissue contrast. Superparamagnetic IONs

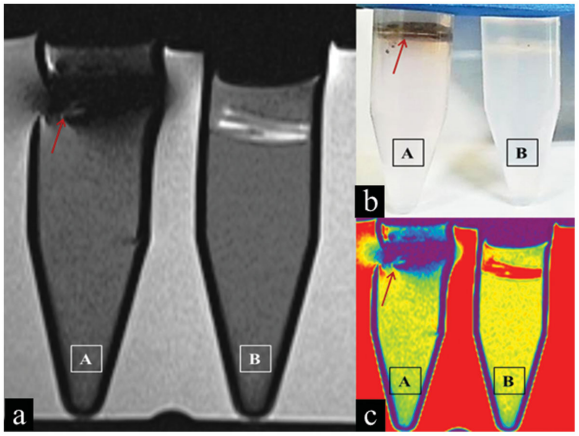


**Figure 10.** T2 contrast image of MADO-Fe3O4 (A) and MADO nanofibers (B): a) MRI image, b) Optical image c) Colour coded image.

(SPIONs) are a T2 contrast agent widely used for MRI contrast imaging.[27] T2 refers to the spin–spin relaxation time of the sample, and T2-weighted images can reveal the presence of superparamagnetic iron centers. SPIONs were utilized here for an experiment that mimics the in-vivo tumor environment. As expected, MADO–$Fe_3O_4$–BTZ nanofiber discs embedded in an agar phantom tube showed marked T2 contrast compared to those in an agar medium and control nanofibers (**Figure 10**). The signal drop is indicated by a red arrow.

## 3. Conclusion

In summary, we successfully developed mussel-inspired electrospun nanofibers capable of binding IONPs and the anticancer drug BTZ for the potential application of hyperthermic chemotherapy. The catechol moieties of the nanofibers were utilized for binding and releasing borate-containing therapeutics such as BTZ in a pH-dependent manner and IONPs for repetitive hyperthermia treatments. Catecholic magnetic nanofibers exhibited an efficient heating ability upon application of an AMF, and a well-maintained cyclic heating performance under the presence of the AMF. In-vitro studies demonstrated that the drug-bound catecholic magnetic nanofibers exhibited an excellent anticancer effect. The MADO–$Fe_3O_4$–BTZ nanofibers can therefore be considered a potential material for cancer therapy that exploits the synergistic effect of hyperthermia and chemotherapy; the anticancer efficiency can be further improved by repeated hyperthermia treatments. This work demonstrates how smart nanofibers can be used for the combined application of hyperthermia and chemotherapy in a single platform.

## 4. Experimental Section

*Materials*: Methacryloyl chloride, sodium borate, sodium bicarbonate, 3,4-dihydroxyphenethylamine hydrochloride, tetrahydrofuran (THF), dimethylformamide (DMF), and methyl methacrylate (MMA) were purchased from Daejung Co. Diethyl ether, methylene chloride, iron(III) acetylacetonate ($Fe(acac)_3$), 1,2-hexadecanediol (90%), oleic acid, oleylamine (70%), benzyl ether (98%), 2-cyano-2-propyl dodecyl

trithiocarbonate (CPDB), azobisisobutyronitrile (AIBN), ethanol, and hexane were purchased from Sigma Aldrich, South Korea.

*Synthesis of Dopamine Methacrylamide (DMA)*: Details of the synthesis of DMA are described in a previous research report by Glass et al.[28,29] The product was a gray powder with a yield of 85%. The structure of the monomer was confirmed by $^1$H-NMR. Deuterated dimethyl sulfoxide (DMSO-$d_6$) was used as a solvent for the pure monomer. $^1$H-NMR (400 MHz, 273 K, DMSO-$d_6$, $\delta$): 6.4–6.6 (3H, m, Ph (phenyl)), 5.5 (1H, d, $CH_2$ = C), 5.25 (1H, d, CH = C–), 3.3 (2H, q, $CH_2$–NH–), 2.5 (2H, tr, $CH_2$–Ph), 1.8 (3H, s, $CH_2$C–).

*Synthesis and Characterization of MADO*: In a 50-mL round-bottom flask, the desired amounts of the two monomers MMA (47 mmol) and DMA monomer (9.4 mmol) were dissolved in dry DMF. Then the calculated volumes of the stock DMF solutions of CPDB and AIBN were added. The ratio of monomer (M) to CPDB, [M]:[CPDB], was 150:1 and the ratio of [CPDB]:[AIBN] was 4:1. The mixture was deoxygenated by nitrogen bubbling for 30 min. The reaction was performed in an oil bath at 70 °C for 17 h. Samples were periodically withdrawn to measure the monomer conversion by $^1$H-NMR. The reaction mixture was added dropwise to 400 mL of diethyl ether under stirring to precipitate the synthesized copolymer. The obtained polymer was dissolved in methylene chloride and precipitated in diethyl ether twice to obtain a pure copolymer. The purified polymer was dried under vacuum until achieving a constant weight. The white solid was obtained with 70% yield. According to the $^1$H-NMR, the resulting molar ratio of DMA to MMA in the copolymer was 1:5. The copolymer had a relatively large weight-averaged molecular weight ($M_w \approx 16\,000$ g mol$^{-1}$) and a fairly narrow molar mass distribution $M_w/M_n$ of 1.2, where $M_n$ is the number-averaged molecular weight. $^1$H-NMR (250 MHz, DMSO-$d_6$, $\delta$): 8.70 (s, 1H, –OH), 8.60 (s, 1H, –OH), 6.6–6.4 (m, 3H, Ar–H (Ar = aryl) ), 3.50 (s, 15H, –O–$CH_3$), 3.24 (m, 2H, Ar-$CH_2$–$CH_2$(NH)–), 2.45 (m, 2H, Ar–$CH_2$–$CH_2$(NH)–), 1.2–0.9 (m, 18H, –C–$CH_3$).

*Synthesis of Iron Oxide Nanoparticles (IONPs)*: The synthesis of iron oxide nanoparticles was carried out as described earlier.[15]

*Fabrication of Catecholic Nanofibers MADO*: Copolymer solutions were prepared by dispersing the polymer at a concentration of 25 wt% in DMF. The obtained solutions were placed in a plastic syringe tube and fed through a metal capillary (nozzle) with an inner diameter of $d_i = 0.21$ mm (21 G) attached to a 1D robot-system that moved laterally and was controlled by the LabVIEW 9.0 software program (National Instrument). The feeding rate was maintained at 0.5 mL h$^{-1}$ via a controllable syringe pump. Electrospinning was carried out at a voltage of 18 kV and working distance of 15 cm at room temperature. Thus obtained nanofibers were vacuum dried for 24 h to remove the residual solvent, and this sample was used for further studies. A comparison of the shear viscosity as a function of shear rates for 25 wt% PMMA solution and 25 wt% MADO measured at room temperature are available in the SI (Figure S1). The pure PMMA solution behaves like a typical shear thinning fluid, with a plateau in viscosity at low shear rates. For MADO, the viscosity is higher due to the interactions between the catecholic groups and solvent.[30]

*Fabrication of Drug-Bound Catecholic Nanofibers MADO–BTZ*: The obtained copolymer solutions (10 mL) along with 2.5 mg (0.1 wt%) of Bortezomib (Santa Cruz Biotechnology, Dallas, USA) were electrospun in the same way as MADO nanofibers with the difference that a feeding rate of 1 mL h$^{-1}$ was used. Thus prepared nanofibers (MADO–BTZ) were vacuum dried for 24 h and kept for further use.

*Fabrication of Catecholic Magnetic Nanofibers MADO–$Fe_3O_4$ and Drug-Bound Catecholic Magnetic Nanofibers MADO–$Fe_3O_4$–BTZ*: In a typical procedure, the obtained electrospun catecholic nanofibers (MADO or MADO–BTZ, 5 cm × 5 cm) weighing around 60 mg were weighed and carefully dipped into the 10 mL of aqueous solution containing 15 wt% $Fe_3O_4$ NPs (with respect to the weight of the nanofibers). In order to utilize the catecholic–metal conjugation, the pH of the aqueous solution was adjusted to 8.5 as an optimum for the present study. The nanoparticles interacted with the surfaces of the MADO nanofibers after increasing the pH, and the color of the fiber mats evolved from white to brown.

*Sample Preparation for Boron-11 NMR Spectroscopy*: Bortezomib (BTZ) and dopamine hydrochloride (DA) were dissolved separately in deuterated DMSO at 0.2 M concentration. The two solutions were mixed to give a stock solution of DA–BTZ conjugate at 0.1 M in DMSO-$d_6$. $D_2O$ was used to dilute the DA–BTZ stock to 1 mM, and the pH of these solutions were adjusted with DCl and NaOD to 5 and 7.4, respectively. For the $^{11}$B-NMR study, between VPBA and catechol, VPBA (4 mg, $3.28 \times 10^{-5}$ mol) and dopamine hydrochloride (140 mg, $73.8 \times 10^{-4}$ mol) was dissolved in $D_2O$, and the pH was adjusted to 7.4 by adding NaOD. In the last solution, same amount of VPBA and dopamine was added except the pH was adjusted to 5.

*Characterization of IONPs and MADO Nanofibers*: Size, morphology, and crystal structure of the as-synthesized $Fe_3O_4$ nanoparticles and MADO–$Fe_3O_4$–BTZ were investigated by TEM (JEOL JEM, Japan) and the corresponding SAED (specific-area electron diffraction; Figure S3, SI). XRD analysis of as-synthesized $Fe_3O_4$ and MADO–$Fe_3O_4$ were carried out by a Rigaku x-ray diffractometer (Cu K$\alpha$, $\lambda = 1.54059$ Å) over Bragg angles ranging from 10° to 90° to study the crystalline structure of the materials (Figure S4, SI). The surface structure and morphology of the as-prepared MADO, $Fe_3O_4$-MADO, and MADO–$Fe_3O_4$–BTZ nanofibers were studied by FESEM (Zeiss Supra 40VP). The elemental composition and surface state of the samples were checked using XPS (AXIS-NOVA, Kratos, Inc.) with an Al K$\alpha$ irradiation source (Figure S5, SI). The bonding configurations of the samples were characterized by means of FTIR using a Paragon 1000 Spectrometer (Perkin Elmer) (Figure S6, SI). A micro-Raman spectroscope (Nanofinder 30) with an argon ion laser at an excitation wavelength of 632.8 nm and IR spectroscope (Tokyo Instrument, INC) were used as a powerful tool to observe and probe the mechanism and configuration of Dopa–metal coordination. Since the samples were sensitive to burning by the laser beam, only weak laser power between 10 and 20 mW could be used for all measurements. Magnetic characterization was carried out on a physical property measurement system (PPMS, model 6000). The mechanical properties of the polymeric solution were tested using a rheometer (Malvern KinexusPro) with a 50 or 20 mm/1° or 2° cone/plate geometry.

*AMF-Induced Heat-Generation Properties and Calculation of SAR*: The hyperthermia properties of MADO (control), $Fe_3O_4$, and MADO–$Fe_3O_4$ samples were studied by measuring the temperature rise of the samples under the application of an AMF using an alternating magnetic field generator (OSH-120-B, OSUNG HITECH, Republic of Korea) at room temperature. The magnetic field strength and frequency were adjusted to be 12.57 Oe and a frequency of 293 kHz, respectively. The power of the heating generator was 5 kW. The water-cooled induction coil is made of copper, with an inner diameter of 60 mm. Magnetic nanoparticles with different concentrations (2, 4, 6, 8, and 10 mg per 1 mL of distilled water) were used to check the hyperthermia properties, and a concentration of 6 mg per mL was optimized for the present study. In a typical procedure, 6 mg of $Fe_3O_4$ suspended in 1 mL of deionized water was placed at the center of the coil, whereas in the case of nanofibers, as-prepared nanofibers attached on the tube-like paper support were placed at the center of the coil and an alternating current (AC) magnetic field was applied. To evaluate the heating characteristics of the samples, type-T thermocouples were attached to the surface of the nanofibers. A real-time data acquisition system (NI-DAQ$^R$, National instrument, USA) was used to automatically record the temperature change of the membranes through a Lab VIEW program. Before each experiment, calibration and stabilization of temperature for 10 min was conducted. The heating efficiency of the as-prepared nanoparticles are quantified by calculating the SAR following the procedure as described earlier.[31] The SAR values were calculated using the equation

$$\mathrm{SAR} = C\left(\frac{\Delta T}{\Delta t}\right)\frac{1}{m_{\mathrm{magn}}}$$

where $C$ is the sample-specific heat capacity, which was calculated as a mass-weighted mean value of magnetite and water. The heat-capacity of magnetite is not taken into account for the current study because of its low concentration, and hence the heat capacity for water (4.18 J g$^{-1}$ K$^{-1}$) was taken as the sample's heat capacity.[32] $\Delta T/\Delta t$ is the initial slope of the time-dependent temperature curve and is obtained for the initial

60 s once after the magnetic field is switched on as the curve follows a linear relationship in this regime. The value of $m_{magn}$ considered as the amount of magnetite per total amount of magnetite and water. Here the volume of water was 1 mL, which is equal to 1 g.

*Biocompatibility Study of Nanofibers*: MADO nanofibers were seeded with $5 \times 10^4$ cells of the NIH3T3 (mouse embryonic fibroblast cells) cell line into 24-well plate and cultured in Dulbecco's Modified Eagle Medium (DMEM) in 5% $CO_2$ incubator at 37 °C in a humidified environment. Nanofibers were taken in triplicate along with the control, which have cells seeded onto the coverslip (SPL Lifesciences, Korea) only. As negative control, 5 μg $mL^{-1}$ triton was added to cells grown on a coverslip in triplicate. After 1, 3, and 5 days, 50 μL MTS reagent (Promega, USA) was added to each of the wells and incubated for 4 h. The absorbance at 490 nm was measured using a microplate reader. For cell attachment studies, the nanofibers were isolated after 5 days and washed with phosphate buffered saline (PBS) 3 times and fixed with 4% PFA (Paraformaldehyde). After drying, the nanofibers were mounted with mounting medium containing DAPI (4′,6-diamidino-2-phenylindole, ProlongGold antifade reagent, Molecular Probes, USA) and visualized in fluorescence microscope (Olympus, USA) using blue/cyan filter (Figure S7, SI).

*Drug Release from MADO–BTZ Nanofiber*: The pH-dependent release of BTZ from the mussel-inspired catecholic nanofibers was carried out to prove the pH-sensitive drug release. We took two buffer solutions at pH 7.4 and 5 to mimic the physiological pH and the acidic pH of tumor environments, respectively. The known amount of drug-bound catechol nanofibrous MADO–BTZ mats were immersed in 5 mL of the prepared two buffer solutions. The tubes were placed in a shaking incubator at 37 °C. The buffer solutions were taken and replaced with fresh solution at predetermined time intervals, and the experiments were done in triplicate. The drug release was determined using UV–vis spectroscopy (HP 8453 UV–vis spectroscopy system, Germany) at 270 nm. The control graph had been already drawn using the known concentrations of drug at 270 nm (Figure S8, SI). Using this control graph, the exact percentage of drug release from the catecholic nanofibers was determined at different pH values.

*In Vitro Anticancer Study*: In vitro hyperthermia studies were carried out using the alternating magnetic field generator (OSH-120-B, OSUNG HITECH, Republic of Korea). The magnetic field strength and frequency were adjusted to be 12.57 Oe and 293 kHz, respectively, to maintain an optimum temperature for the hyperthermia treatment. In a typical experiment, MADO (control), MADO–$Fe_3O_4$, MADO–BTZ, and MADO–$Fe_3O_4$–BTZ nanofibers were seeded ($5 \times 10^4$ cells) with the MCF-7 (human breast cancer) and 4T1 (mouse mammary carcinoma) cell lines in a 24-well plate and cultured in DMEM at 5% $CO_2$ incubator at 37 °C in a humidified environment. All samples were taken in triplicate. Warm PBS wash was given to each sample after 24 h of incubation. Initially, we separated the samples into treated (with hyperthermia) and untreated groups (without hyperthermia) before the experiment. For testing the hyperthermia effect on the cells, the AMF was turned 'on' at day 1 after seeding the cancer cells. The cell viability was measured using a MTS assay. The treated group received hyperthermia treatment for 10 min in a sterile environment whereas untreated samples were isolated into a mini-petri dish for the same period of time thereby cancelling out environmental effects on cell death. After hyperthermia treatment of all samples, fresh DMEM was added and incubated in a 24-well plate again for 24 h in a 5% $CO_2$ incubator at 37 °C in a humidified environment and then 50 μL of MTS reagent was added to each of the wells and incubated for another 4 h. The absorbance at 490 nm was measured using a microplate reader. In order to check the intensified anticancer efficacy of MADO–$Fe_3O_4$–BTZ due to the repeated hyperthermia treatments, the same experiments were carried out again on day 2 and 3. The cell viabilities were evaluated using an MTS assay 24 h after hyperthermia treatments.

*Live/Dead Assay*: A MADO–$Fe_3O_4$–BTZ nanofiber was seeded with $5 \times 10^4$ cells (4T1) in a 24-well plate and cultured in DMEM in a 5% $CO_2$ incubator at 37 °C in a humidified environment. After one day incubation, the MADO–$Fe_3O_4$–BTZ nanofiber was isolated, washed with warm PBS three times and was subjected to hyperthermia treatment for 10 min. After hyperthermia, the MADO–$Fe_3O_4$–BTZ nanofiber was treated with 200 μL of calcein AM (4 μM) and ethidium homodimer (0.5 μM) dissolved in PBS for 30 min at room temperature. MADO–$Fe_3O_4$–BTZ was directly viewed under a fluorescent microscope with a standard fluorescein band pass filter for calcein and a Texas Red dye filter for the ethidium homodimer. The same procedure was used after the hyperthermia treatments on day 1, 2, and 3.

## Supporting Information

Supporting Information is available from the Wiley Online Library or from the author.

## Acknowledgements

A.G. and A.R.K.S. contributed equally to this work. This research was supported by grants from the Basic Science Research Program through the National Research Foundation of Korea (NRF), funded by the Ministry of Education, Science and Technology (Project no. 2013R1A2A2A04015484). The authors would like to thank the staff of the CBNU central lab, Mr. Yeon-Soo Han, Ms. Eunjeong Shin, and Mr. Jong-Gyun Kang for help with NMR, FESEM and TEM.

Received: January 30, 2015
Revised: March 5, 2015
Published online: March 30, 2015

[1] a) Y. Dong, W. K. K. Wu, C. W. Wu, J. J. Y. Sung, J. Yu, S. S. M. Ng, *Brit. J. Cancer* **2011**, *104*, 893; b) J. H. Maeng, D. H. Lee, K. H. Jung, Y. H. Bae, I. S. Park, S. Jeong, Y. S. Jeon, C. K. Shim, W. Kim, J. Kim, J. Lee, Y. M. Lee, J. H. Kim, W. H. Kim, S. S. Hong, *Biomaterials* **2010**, *31*, 4995; c) J. L. Arias, B. Clares, M. E. Morales, V. Gallardo, M. A. Ruiz, *Curr. Drug Targets* **2011**, *12*, 1151; d) M. M. Yallapu, S. F. Othman, E. T. Curtis, B. K. Gupta, M. Jaggi, S. C. Chauhan, *Biomaterials* **2011**, *32*, 1890.
[2] C. B. Huang, S. J. Soenen, J. Rejman, J. Trekker, C. X. Liu, L. Lagae, W. Ceelen, C. Wilhelm, J. Demeester, S. C. De Smedt, *Adv. Funct. Mater.* **2012**, *22*, 2479.
[3] Y. J. Kim, M. Ebara, T. Aoyagi, *Adv. Funct. Mater.* **2013**, *23*, 5753.
[4] S. H. Wang, C. Wang, B. Zhang, Z. Y. Sun, Z. Y. Li, X. K. Jiang, X. D. Bai, *Mater. Lett.* **2010**, *64*, 9.
[5] H. S. Yoo, T. G. Kim, T. G. Park, *Adv. Drug Delivery Rev.* **2009**, *61*, 1033.
[6] A. Amarjargal, L. D. Tijing, C. H. Park, I. T. Im, C. S. Kim, *Eur. Polym. J.* **2013**, *49*, 3796.
[7] T. C. Lin, F. H. Lin, J. C. Lin, *Acta Biomater.* **2012**, *8*, 2704.
[8] B. P. Lee, P. B. Messersmith, J. N. Israelachvili, J. H. Waite, *Annu. Rev. Mater. Res.* **2011**, *41*, 99.
[9] H. Y. Son, J. H. Ryu, H. Lee, Y. S. Nam, *Macromol. Mater. Eng.* **2013**, *298*, 547.
[10] B. Mizrahi, S. A. Shankarappa, J. M. Hickey, J. C. Dohlman, B. P. Timko, K. A. Whitehead, J. J. Lee, R. Langer, D. G. Anderson, D. S. Kohane, *Adv. Funct. Mater.* **2013**, *23*, 1527.
[11] C. K. Poh, Z. L. Shi, T. Y. Lim, K. G. Neoh, W. Wang, *Biomaterials* **2010**, *31*, 1578.
[12] J. S. Choi, P. B. Messersmith, H. S. Yoo, *Macromol. Biosci.* **2014**, *14*, 270.
[13] a) R. Liu, Y. L. Guo, G. Odusote, F. L. Qu, R. D. Priestley, *ACS Appl. Mater. Interfaces* **2013**, *5*, 9167; b) J. W. Cui, Y. Yan, G. K. Such, K. Liang, C. J. Ochs, A. Postma, F. Caruso, *Biomacromolecules* **2012**, *13*, 2225.

[14] J. Su, F. Chen, V. L. Cryns, P. B. Messersmith, *J. Am. Chem. Soc.* **2011**, *133*, 11850.
[15] J. Xie, S. Peng, N. Brower, N. Pourmand, S. X. Wang, S. H. Sun, *Pure Appl. Chem.* **2006**, *78*, 1003.
[16] a) A. GhavamiNejad, S. Hashmi, H. I. Joh, S. Lee, Y. S. Lee, M. Vatankhah-Varnoosfaderani, F. J. Stadler, *PhysChemChemPhys* **2014**, *16*, 8675; b) I. Savva, D. Constantinou, O. Marinica, E. Vasile, L. Vekas, T. Krasia-Christoforou, *J. Magn. Magn. Mater.* **2014**, *352*, 30.
[17] M. J. Harrington, A. Masic, N. Holten-Andersen, J. H. Waite, P. Fratzl, *Science* **2010**, *328*, 216.
[18] a) N. Holten-Andersen, M. J. Harrington, H. Birkedal, B. P. Lee, P. B. Messersmith, K. Y. C. Lee, J. H. Waite, *Proc. Natl. Acad. Sci. USA* **2011**, *108*, 2651; b) I. Michaudsoret, K. K. Andersson, L. Que, *Biochemistry* **1995**, *34*, 5504.
[19] H. B. Zeng, D. S. Hwang, J. N. Israelachvili, J. H. Waite, *Proc. Natl. Acad. Sci. USA* **2010**, *107*, 12850.
[20] J. Yu, W. Wei, M. S. Menyo, A. Masic, J. H. Waite, J. N. Israelachvili, *Biomacromolecules* **2013**, *14*, 1072.
[21] W. Scarano, H. X. Lu, M. H. Stenzel, *Chem. Commun.* **2014**, *50*, 6390.
[22] P. Guardia, R. Di Corato, L. Lartigue, C. Wilhelm, A. Espinosa, M. Garcia-Hernandez, F. Gazeau, L. Manna, T. Pellegrino, *ACS Nano* **2012**, *6*, 3080.
[23] S. H. Noh, W. Na, J. T. Jang, J. H. Lee, E. J. Lee, S. H. Moon, Y. Lim, J. S. Shin, J. Cheon, *Nano Lett.* **2012**, *12*, 3716.
[24] a) S. Laurent, D. Forge, M. Port, A. Roch, C. Robic, L. V. Elst, R. N. Muller, *Chem. Rev.* **2008**, *108*, 2064; b) A. Ito, M. Shinkai, H. Honda, T. Kobayashi, *J. Biosci. Bioeng.* **2005**, *100*, 1.
[25] a) S. H. Ku, C. B. Park, *Biomaterials* **2010**, *31*, 9431; b) S. H. Ku, J. Ryu, S. K. Hong, H. Lee, C. B. Park, *Biomaterials* **2010**, *31*, 2535.
[26] a) Y. Qu, J. B. Li, J. Ren, J. Z. Leng, C. Lin, D. L. Shi, *Nanoscale* **2014**, *6*, 12408; b) J. P. May, S. D. Li, *Expert Opin. Drug Delivery* **2013**, *10*, 511.
[27] R. Thomas, I. K. Park, Y. Y. Jeong, *Int. J. Mol. Sci.* **2013**, *14*, 15910.
[28] P. Glass, H. Y. Chung, N. R. Washburn, M. Sitti, *Langmuir* **2009**, *25*, 6607.
[29] M. Vatankhah-Varnoosfaderani, S. Hashmi, A. GhavamiNejad, F. J. Stadler, *Polym. Chem. UK* **2014**, *5*, 512.
[30] M. Vatankhah-Varnoosfaderani, A. GhavamiNejad, S. Hashmi, F. J. Stadler, *Macromol. Rapid. Commun.* **2015**, *36*, 447.
[31] P. Drake, H. J. Cho, P. S. Shih, C. H. Kao, K. F. Lee, C. H. Kuo, X. Z. Lin, Y. J. Lin, *J. Mater. Chem.* **2007**, *17*, 4914.
[32] R. Ghosh, L. Pradhan, Y. P. Devi, S. S. Meena, R. Tewari, A. Kumar, S. Sharma, N. S. Gajbhiye, R. K. Vatsa, B. N. Pandey, R. S. Ningthoujam, *J. Mater. Chem.* **2011**, *21*, 13388.